Int. J. Electrochem. Sci., 16 **(2021)** Article Number: 211244, doi: 10.20964/2021.12.36

International Journal of
ELECTROCHEMICAL
SCIENCE
www.electrochemsci.org

Effect of dealloying parameters on HER electrocatalytic performance of nanoporous silver

Zi-jun Zhao[1], *Wen-feng Yu*[1], *Hui-yao Liu*[1], *Xin-yi Liu*[1], *Xu Wang*[1,2,*], *Ming Wu*[1]

[1] School of Mechanical Engineering, Liaoning Petrochemical University, Fushun 113001, Liaoning, China
[2] Department of Materials Science & Engineering; Hong Kong Institute for Advanced Study, City University of Hong Kong, Kowloon, Hong Kong
[*]E-mail: wx1979875@hotmail.com

Received: 6 September 2021 / *Accepted:* 11 October 2021 / *Published:* 10 November 2021

$Ag_{15}Cu_{85}$ binary alloy ribbon, as the precursor, was executed high-temperature oxidation at 650 ℃ and dealloying with different durations to fabricate nanoporous silver at different stages. The HER electrocatalytic performance of nanoporous silver at different stage was tested using open circuit potential (OCP), linear sweep voltammetry (LSV), and potential polarization curve. The results show that the nonporous silver electrode in the B1 stage has the best anti-toxic performance, Ecorr is -0.088V, and the icorr is 1.2×10^{-7} A/cm^2; the nanoporous silver electrode in the A2 stage shows the lowest Tafel slope (45.8 mV dec^{-1}); at a current density of 10 mA/cm^2, the hydrogen evolution overpotential of the nanoporous silver electrode in the B3 stage is 37.6 mV. From all those electrochemical tests, the nanoporous silver electrode in the B1 stage exhibited the best comprehensive HER performance.

Keywords: nanoporous silver; hydrogen evolution performance; high-temperature oxidation; dealloying

1. INTRODUCTION

The most important factor of the sustainable development of humanity is energy [1-5]. Recently, with the development of the human race, the pollution caused by fossil energy becomes severe increasingly. Additionally, the production of fossil energy decreased day by day [6]. In this case, clean energy such as solar energy, wind energy, and tidal energy are exploited. However, that kind of clean energy could not be matched well between supply and demand due to the intermittency and volatility. Therefore, new types of clean energy with stable supply are explored.

Hydrogen energy with high calorific value and high energy density is the most valuable competitor in plenty of clean energy. Hydrogen, as a reaction product of fuel cells, produces only water after combustion, which does not produce greenhouse gases. Moreover, hydrogen, as the ideal energy in the future, could be produced by the electrolysis of water. Consequently, hydrogen energy, as a strong competitor in the energy field, would be widely employed in the future. Moreover, electrolyze water to produce hydrogen is considered the vintage pathway to 'hydrogen economy' [7,8]. However, the hydrogen production efficiency in the cathode hydrogen evolution reaction (HER) of water electrolysis is inseparable from factors such as hydrogen evolution overpotential, current density, electrode material, and operating temperature. Therefore, a suitable HER electrocatalyst will become an effective strategy to improve hydrogen production efficiency [9]. According to the currently known HER electrocatalysts, the Pt-based catalyst has the highest catalytic efficiency. However, the natural reserves of Pt are small, and the price is high. Therefore, cheaper catalysts for replacing Pt have become a hot spot in this field. In recent years, nanoporous materials have shown excellent performance in catalysis, energy storage, sensing, *etc.*, due to their high specific surface area and interface [10-16]. There are few reports on the research of nanoporous metals in HER catalysis. In our previous work, we found that ultrasonic irradiation could tune the dealloying process and microstructure of nanoporous silver [17]. However, the distribution of ligament and pore size is not even, which might lead a bad effect on electrocatalytic performance. Thus, a new strategy, high-temperature oxidation pretreatment, is developed to fabricate superior HER electrocatalysts.

This paper takes nanoporous silver (NPS) as the research object. Dealloying and high-temperature oxidation parameters were modified to control the nanoporous structure and fabricate nanoporous silver electrodes at different stage. Nanoporous silver electrode at different stage was used as the working electrode to test the HER performance. and prepares nanoporous silver in different conditions by controlling the dealloying time and high-temperature oxidation pretreatment time. Comparing the catalytic performance of nanoporous silver in different states in HER provides a theoretical basis for the preparation of high-efficiency HER electrocatalysts.

2. EXPERIMENTAL

The specimens, as the working electrode, was fabricated by dealloying $Ag_{15}Cu_{85}$ alloy ribbon, which was designed as the precursor alloy.

The $Ag_{15}Cu_{85}$ precursor alloys ribbon, with a thickness of ~60 μm, were cut into 10mm × 10mm. In addition, before the dealloying process the precursors were oxidized at 650 ℃ with the duration of 1 min, 3 min and 5 min, respectively. Moreover, the dealloying process was executed in a constant temperature water bath. The dealloying medium used in this research was 5 % aqueous nitric acid, and the dealloying temperature was 45 ℃. The dealloying duration was divided into three different conditions to explore the effect of dealloying duration on HER catalytic performance. Additionally, the dealloying products were the working electrodes in the HER test. The fabrication process of NPS at different stages is shown in Table 1. Besides, the scanning electron microscope (FEI QUANTA 450) equipped with an energy dispersive X-ray spectrometer (EDS) were used to characterize the morphology of the oxidized ribbon and de-alloyed ribbon.

Table 1 fabricating condition of NPS

Numbering	Temperature of oxidation (HTO) (℃)	Oxidation duration (min)	Dealloying duration (min)
A1			15
A2		1	30
A3			60
B1			15
B2	650	3	30
B3			60
C1			15
C2		5	30
C3			60

The electrocatalyst performance was investigated in a three-electrode system. The working electrodes were cleaned in absolute ethanol and dried in a constant temperature drying oven before the electrochemistry test. The electrochemistry tests were carried out in Corrtest electrochemical workstation. Commercial Pt was selected as the counter electrode; saturated calomel electrode was selected as the reference electrode. The electrolyte solution was 0.5M/L nitrogen-saturated sulfuric acid aqueous solution. The scanning speed of linear sweep voltammetry and dynamic potential polarization were 5 mV/s and 0.5 mV/s, respectively.

3. RESULTS and DISCISSION

3.1 Morphology characterization

Figure 1 showed the SEM image of $Ag_{15}Cu_{85}$ alloy ribbon after high-temperature oxidation with different durations. When the high-temperature oxidation process lasted for 1 min, island oxides appeared on the surface of the alloy ribbon, as shown in Fig 1(a). As the oxidation time increases, the area of island oxidation increases gradually, as shown in Fig 1(b-c). It can be seen from the EDS results that the main components of the island oxide formed on the surface of the alloy ribbon are Cu and O. According to the atomic ratio, the oxides on the surface are CuO and Cu_2Orespectively. In addition, there are unevenly precipitated Ag particles on the surface of the oxide film, as shown in Fig. 1(a).

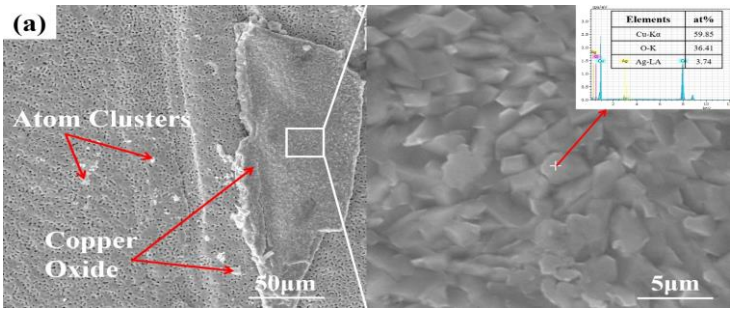

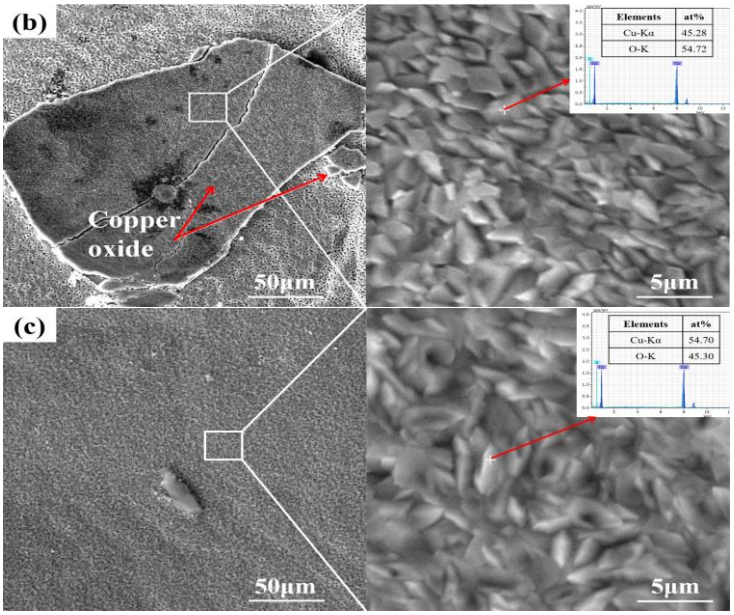

Figure 1. SEM images of $Ag_{15}Cu_{85}$ ribbon under 650 ℃ oxidization with different durations: (a) 1 min, (b) 3 min, and (c) 5 min. The EDS results are illustrated.

Figure 2 showed the SEM morphologies of alloy ribbons under high-temperature oxidation with different durations being de-alloyed for 15 min, 30 min, and 60 min, respectively. The alloy ribbons after high-temperature oxidation with different durations exihibited different sizes and three-dimensional ligament/pore structure NPS in the initial stage of dealloying. With the extension of oxidation time, the size of the ligament of NPS increased significantly, as shown in Fig. 2(a, d, g). As the dealloying process continues, the uniformity of nanoporous silver ligaments/pores prepared from alloy ribbons with different high-temperature oxidation times have changed significantly. For the alloy ribbon under the same high-temperature oxidation duration, the nanoporous silver ligament/pore structure obtained after dealloying for 1 hour was the most uniform. In addition, the uniformity of the ligaments/pores obtained after dealloying was affected by the high-temperature oxidation duration. The nanoporous silver fabricated from the alloy ribbon under the high-temperature oxidation for three minutes exhibited an ultra-uniform ligament/pore structure at the same dealloying time, as shown in Fig. 2(d-f). The island oxide layer has an impact on the ligament/pore structure during the dealloying process.And the precursor undergoes a suitable high-temperature oxidation pretreatment would form a more uniform ligament/pore structure which might be beneficial for electrocatalytic performance during the dealloying process.

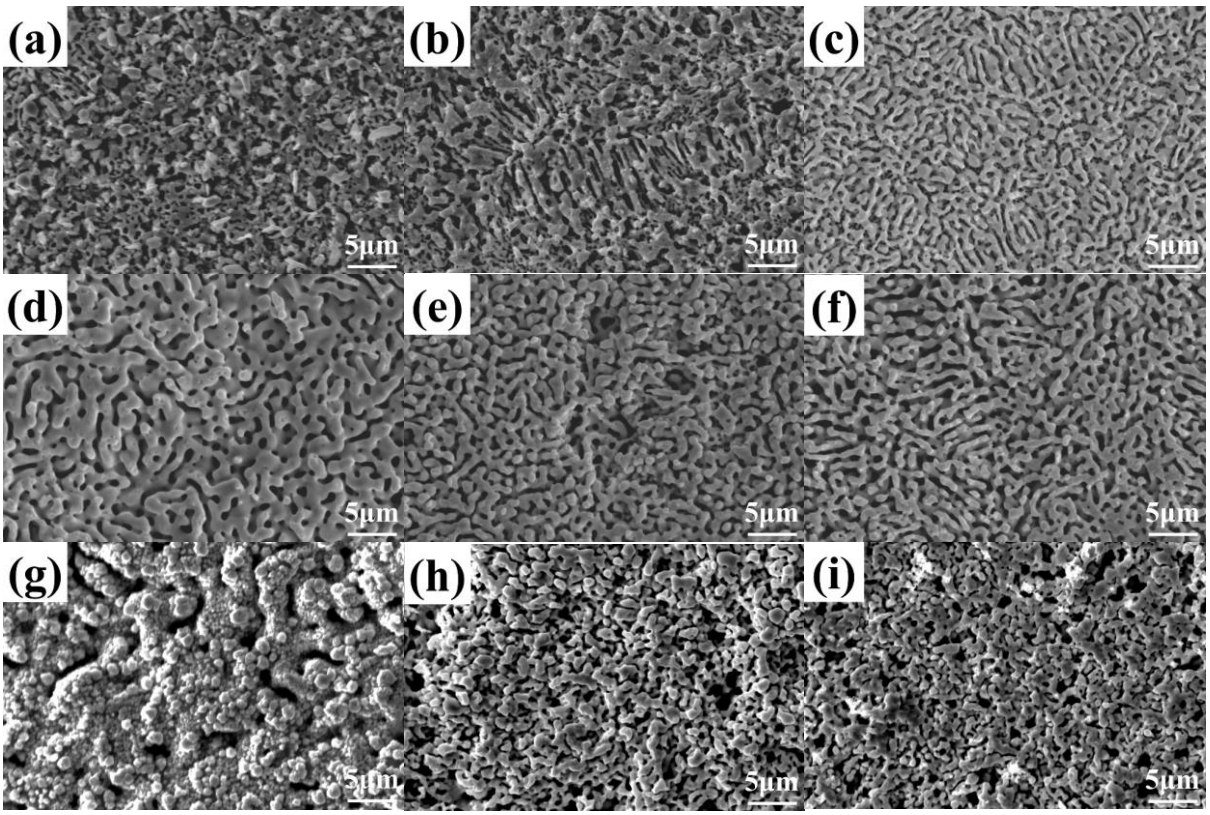

Figure 2. SEM images of high-temperature oxidation (HTO) pretreatment $Ag_{15}Cu_{85}$ ribbons de-alloyed at 45 ℃, 5% HNO_3 with different durations, HTO 1 min: (a) 15 min, (b) 30 min, (c) 60 min; HTO 3 min: (d) 15 min, (e) 30 min, (f) 60 min; HTO 5 min: (g) 15 min, (h) 30 min, (i) 60 min.

3.2 Corrosion resistance test

Figure 3 showed the open circuit potential (OCP) curves of NPS in different states. As we all know, the OCP curve is the relationship between corrosion potential and immersion time. In a 0.5M/L sulfuric acid aqueous solution saturated with nitrogen, the OCP curves of NPS in different states gradually stabilized, which indicates that a passivation layer (usually an oxide) was formed during the test. After being immersed in a 0.5M/L sulfuric acid aqueous solution saturated with nitrogen for 900 s, the OCP values of NPS in different states were not much different except C3. The OCP value of NPS prepared after 1 min and 3 min high-temperature oxidation did not change significantly with the extension of dealloying time. The OCP value of NPS prepared after 5 min high-temperature oxidation has changed significantly with the increase of dealloying time, which indicates that the high-temperature oxidation process will affect the electrical properties of NPS.

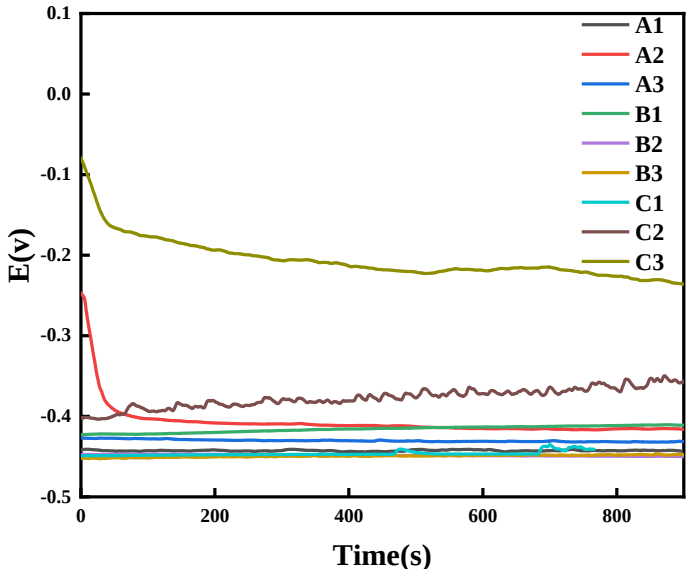

Figure 3. The OCP curves of different stage nanoporous silver at N_2 saturated 0.5M/L H_2SO_4 aqueous solution.

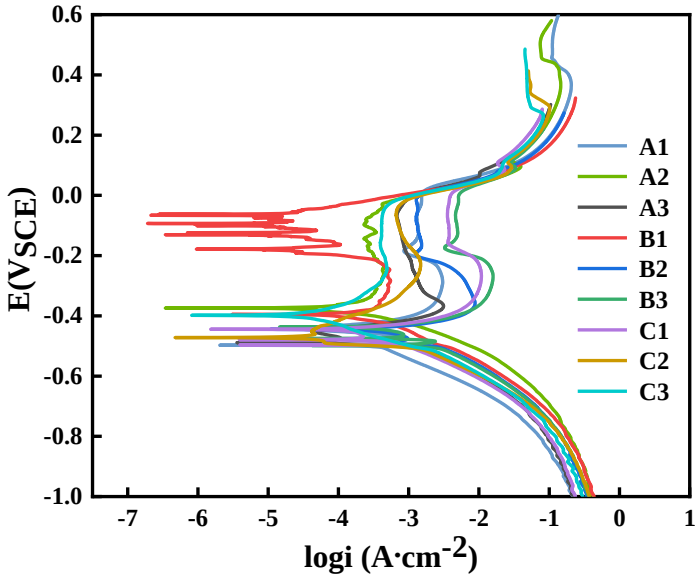

Figure 4. Polarization curves of different stage nanoporous silver at N_2 saturated 0.5M/L H_2SO_4 aqueous solution.

Figure 4 showed the potentiodynamic polarization curves of NPS at different stages in a 0.5M/L nitrogen-saturated H_2SO_4 solution. In order to study the anti-toxicity of NPS electrocatalysts at different stages, the fitted results of polarization curves were recorded in Table 2. According to the corrosion kinetics, the corrosion tendency of material was related to the self-corrosion potential (Ecorr) of the material itself. The lower the Ecorr of the material, the greater the corrosion tendency of the material. According to the fitted results (Table 2), when the high-temperature oxidation condition and the dealloying time were the same, A2, B1, and C3 all exhibited higher Ecorr. In addition, the NPS in the B1 stage exhibited a very high self-corrosion potential, and the corrosion current density (icorr) was 2-

4 orders of magnitude lower than that of the samples in other crafts, which showed that the samples in the B1 stage are better than those in other stages. In the same way, the anti-drug ability was stronger.

Table 2 Electrochemical parameters of nanoporous silver at different stage

Numbering	i_{corr} (A/cm^2)	E_{corr} (V_{SCE})
A1	1.5×10^{-5}	-0.491
A2	5.3×10^{-4}	-0.374
A3	6.7×10^{-5}	-0.488
B1	1.2×10^{-7}	-0.088
B2	7.8×10^{-4}	-0.445
B3	1.8×10^{-3}	-0.498
C1	4.9×10^{-5}	-0.424
C2	5.6×10^{-5}	-0.472
C3	8.8×10^{-5}	-0.398

3.2 Catalytic performance of NPS electrode in different stages for HER

Figure 5 showed the Tafel curve of NPS at different stages in a 0.5M/L nitrogen-saturated H_2SO_4 solution.

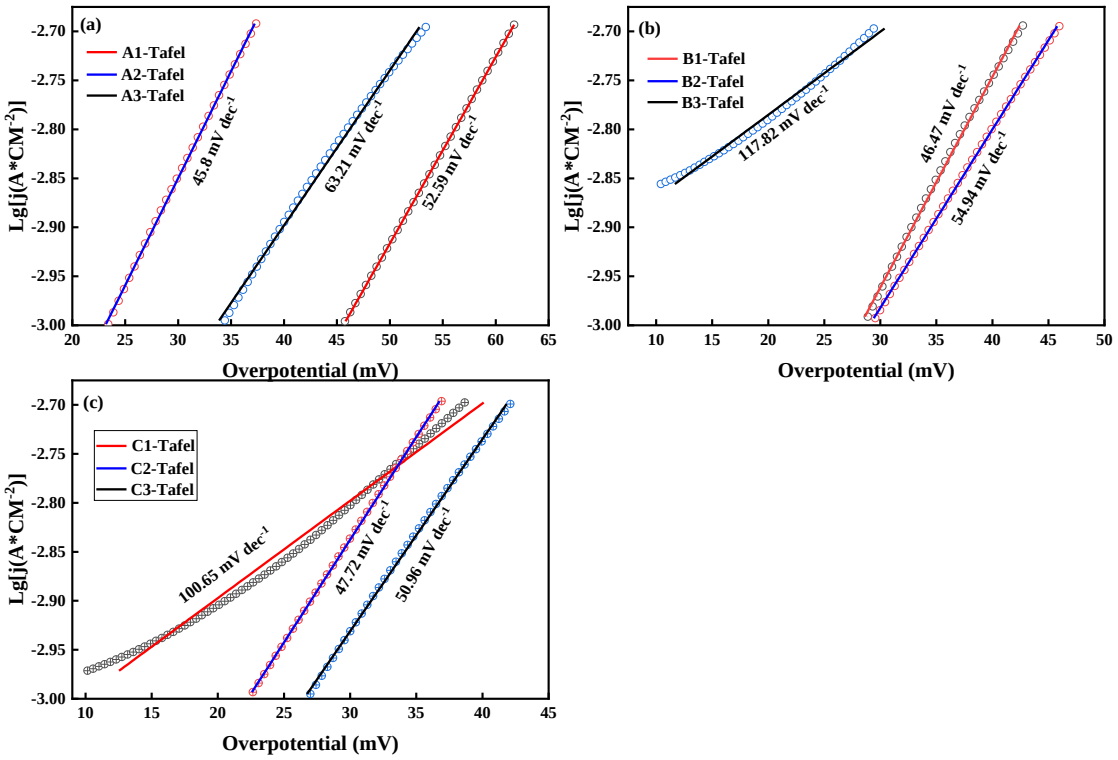

Figure 5. Tafel slope of different stage nanoporous silver at N_2 saturated 0.5M/L H_2SO_4 aqueous solution.

It is obvious from Fig. 5(a) that with the extension of the dealloying time, the Tafel curve shifted to lower hydrogen evolution overpotential under the high-temperature oxidation of 1 min. The results showed that the extension of dealloying time was beneficial to improve the catalytic activity of the electrode. As is shown in Fig. 5(b), when the high-temperature oxidation was 3 minutes, with the extension of the dealloying time, the Tafel curve first shifted to the higher hydrogen evolution overpotential. It then moved to the lower hydrogen evolution overpotential. As can be seen from the result of Fig. 5(c), with the extension of dealloying time at high-temperature oxidation for 5 minutes, the Tafel curve gradually shifted to higher hydrogen evolution overpotential first, and then moved to lower hydrogen evolution overpotential, which indicates that the extension of high-temperature oxidation time would decrease the catalytic activity of the electrode.

The linear sweep voltammetry (LSV) curves of NPS at different stages in a 0.5M/L nitrogen-saturated H_2SO_4 solution were shown in Fig. 6(a). It can be seen from the results of LSV test shown in Fig. 6(a) that the hydrogen evolution overpotential of the NPS sample after dealloying for 15 minutes(C1) is the lowest than that of other NPS electrode at the same current density under high-temperature oxidation for 5 min. When the high-temperature oxidation duration was 1 min and 3 min, the hydrogen evolution overpotential of the NPS sample exhibited the same hydrogen evolution overpotential at the same dealloying duration under the current density range of 0 -50 mA/cm^{-2}. In addition, under the same current density, the hydrogen evolution overpotential of B1 was the lowest than that of others, which means that the catalytic activity of the B1 electrode is the highest in this research. Hydrogen evolution overpotential was the main factor that affects the H adsorption and desorption process. Lower hydrogen evolution overpotential would make the H adsorption and desorption process easier to occur, accelerate the reaction speed and improve the efficiency of hydrogen evolution.

Figure 6(b) showed the comparison of the hydrogen evolution performance between NPS electrode, with the best HER performance, fabricated in this work and the reported electrocatalytic performance of representative acid media under the 0.5M/L H_2SO_4 aqueous solution condition. When the current density was 10 mA cm^{-2}, the hydrogen evolution overpotential of the NPS electrode prepared in this work was between 1/2-1/5 of the reported hydrogen evolution electrocatalyst. The results showed that the hydrogen evolution overpotential of NPS was lower than most of the reported electrocatalysis introduced in this work, which means that the NPS electrodes were more conducive to the adsorption and desorption of H^+. In addition, the Tafel slopes of NPS at different stages were not much different from the reported acidic hydrogen evolution electrocatalysts except the NPS electrodes fabricated under B3 and C1 conditions. The Tafel slope of other NPS electrodes were all between 45 mV dec^{-1} - 65 mV dec^{-1}. Although the NPS electrocatalyst with the best hydrogen evolution reaction performance, fabricated in this work was not as good as the commercial Pt reported in the research [18,19], it was slightly better than most of the reported hydrogen evolution electrocatalysts shown in Fig. 6(b) [20-35]. The results indicated that the hydrogen evolution electrocatalysis efficiency of NPS electrodes would have higher electrocatalytic activity.

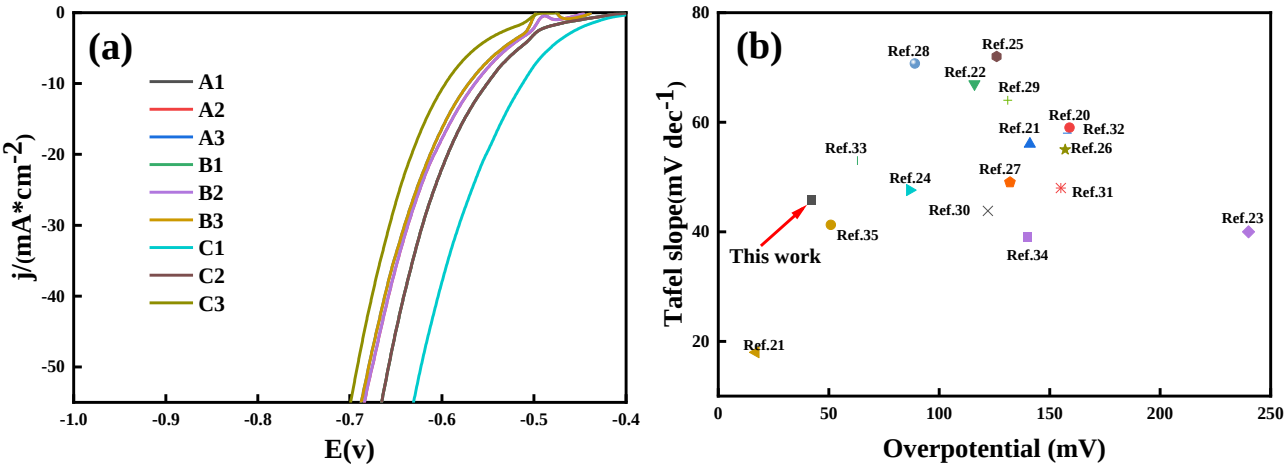

Figure 6. (a) LSV curves of different stage nanoporous silver at N_2 saturated 0.5M/L H_2SO_4 aqueous solution, (b) comparison of HER performance between nanoporous silver at different stage and other HER electrocatalysts under 0.5M/L H_2SO_4 aqueous solution condition.

4. CONCLUSIONS

This work takes the $Ag_{15}Cu_{85}$ alloy ribbon as the research object. After high-temperature oxidation treatment at 650 ℃ for different times, the ally ribbon was executed dealloying process with a duration between 15 min – 60min to fabricate nanoporous silver electrode. Then, the NPS electrode was tested in a 0.5M/L nitrogen-saturated H_2SO_4 solution. The conclusions are as follows.

After the $Ag_{15}Cu_{85}$ alloy ribbon is oxidized at high-temperature, island oxides are produced on the surface. With the extension of the high-temperature oxidation duration, the island oxide on the surface gradually grows up.

The precursor alloy, after high-temperature oxidation, exhibited different kinds of nanoporous structures during the dealloying process. When the high-temperature oxidation is 3 min, the nanoporous structure obtained by dealloying is more uniform.

The different stages of nanoporous silver electrodes obtained after dealloying exhibited different electrochemical performances. The NPS electrode fabricated by A2 condition showed the lowest Tafel slope (45.8 mV dec^{-1}), and the NPS electrode fabricated B1 condition exhibited the strongest anti-toxic performance, the NPS electrode fabricated C1 condition exhibited the lowest hydrogen evolution overpotential. In general, the NPS electrode fabricated B1 condition exhibited superior comprehensive performance.

ACKNOWLEDEGMENT
The authors gratefully acknowledge the sponsorship from National Nature Science Foundation of China, under the project no. 51574147, Liaoning Province Nature Science Foundation, under the project no. 201602474, Scientific Research Project of the Education Department of Liaoning Province, under the project no.2021-LGKZ0388.

References

1. J. Zhang, X. Li, Y. Liu, Z. Zeng, X. Cheng, Y. Wang, W. Tu and M. Pan, *Nanoscale*, 10(2018)11997.
2. G. C. Li, W Sun, Y Lv, G. H. Cheng, Y. M. Chen and G. H. Huang, *Stoch. Env. Res. Risk. A*, 32(2018)2093.
3. P. Wang, Z. Pu, Y. Li, L. Wu, Z. Tu, M. Jiang, Z. Kou, I. S. Amiinu and S. Mu, *ACS Appl. Mater. Inter.*, 9(2017)26001.
4. R. R. Karasani, V. B. Borghate, P. Meshram, H. Suryawanshi and S. Sabyasachi, *IEEE Trans. Power Electron.*, 32(2017)1070.
5. Y. T. Liu, J. Zhang, X. X. Li, Z. W. Zeng, X. Cheng, Y. D. Wang and M. Pan, *Int. J. Electrochem. Sci.,* 14(2019)6123.
6. Z. W. Seh, J. Kibsgaard, C. F. Dickens, I. Chorkendorff, J. K. Nørskov and T. F. Jaramillo, *Science,* 355(2017)4998.
7. M. I. Hoffert, *Soc Sci Q*,73(2006)981.
8. M. H. Ahmadi, A. H. Mohammadi and Dehghani S, *Energy Convers. Manag.,* 76(2013)561.
9. D. T. Hijikata, *Int. J. Hydrog. Energy,* 27(2002)115.
10. T. Fujita, *Sci Technol Adv Mater*, 18(2017)724.
11. J. Erlebacher, M. J. Aziz, A. Karma, N. Dimitrov and K. Sieradzki, *Nature*, 410(2001)450
12. R. Mao, S. H. Liang, X. H. Wang, Q. Yang and B. B. Han, *Corros Sci*, 60(2012)231.
13. A. Wittstock, V. Zielasek, J. Biener, C. M. Friend and M. Bäumer, *Science*, 327(2010)319.
14. X. W. Guo, J. H. Han, P. Liu, L. Y. Chen, Y. Ito, Z. L. Jian, T. N. Jin, A. Hirata, F. J. Li, T. Fujita, N. Asao, H. S. Zhou and M. W. Chen, *Sci. Rep.*, 6(2016)19.
15. M. Shaban, S. Ali and M. Rabia, *J. Mater. Res. Technol.*, 8(2019)4510.
16. J. Wang, L. You, Z. B. Li, X. J. Liu, R. Li, Q. Du, X. Z. Wang, H. Wang, Y. Wu, S. H Jiang and Z. P. Lu, *J. Mater. Sci. Technol.*, 73(2021)145.
17. R. W. Zhang, X. Wang, J. C. Huang, F. Li, Z. Z. Zhang and M. Wu, *RSC Adv*, 9(2019)9937.
18. M. Q. Wang, C. Ye, S. J. Bao, Z. Y. Chen, H. Liu and M. W. Xu, *ChemCatChem*, 9(2017)4169.
19. C. Ye, M. Q. Wang, G. Chen, Y. H. Deng, L. J. Li, H. Q. Luo and N. B. Li, *J. Mater. Chem. A*, 5(2017)7791.
20. M. J. Liu and J. H. Li, *ACS Appl. Mater. Interfaces*, 8(2016)2158.
21. Y. Y. Chen, Y. Zhang, W. J. Jiang, X. Zhang, Z. H. Dai, L. J. Wan and J. S. Hu, *ACS Nano,* 10(2016)8851.
22. L. Wan, J. F. Zhang, Y. Q. Chen, C. Zhong, W. B. Hu and Y. D. Deng, *J. Mater. Sci.*, 52(2017)804.
23. Y. Xu, R. Wu, J. F. Zhang, Y. M. Shi and B. Zhang, *ChemComm*, 49(2013)6656.
24. C. R. Pi, Z. Y. Zhao, X. M. Zhang, B. Gao, Y. Zheng, P. K. Chu, L. J. Yang and K. F. Huo, *Chem. Eng. J.*, 416(2021)129130.
25. X. Zhang, Z. Zhu, X. Liang, F. Ma, J. Zhang, Y. Tan, Z. Pan, Y. Bo and C. Wu, *Chem.Eng. J.*, 408(2020)127270.
26. H. Yan, Y. Xie, Y. Jiao, A. Wu, C. Tian, X. Zhang, L. Wang and H. Fu, *Adv. Mater*., 30(2017)1704156.
27. H. Yang, X. Chen, G. Hu, W. Chen, S. Bradley, W. Zhang, G. Verma, T. Nann, D. Jiang, P.E. Kruger, X. Wang, H. Tian, G. Waterhouse, S. Telfer and S. Ma, *Chem. Sci.*, 11(2020)3523.
28. J. Xiong, J. Li, J. W. Shi, X. L. Zhang, N. T. Suen, Z. Liu, Y. J. Huang, G. X. Xu, W. W. Cai, X. R. Lei, L. G. Feng, Z. H. Yang, L. Huang and H. S. Cheng, *ACS Energy Lett.,*3(2018)341.
29. L. Jia, C. Li, Y. Zhao, B. Liu, S. Cao, D. Mou, T. Han, G. Chen and Y. Lin, *Nanoscale,* 11(2019)23318.
30. C. Huang, X. Miao, C. Pi, B. Gao, X. Zhang, P. Qin, K. Huo, X. Peng and P. K. Chu, *Nano Energy,* 60(2019)520.
31. X. Zhang, J. Wang, T. Guo, T. Liu, Z. Wu, L. Cavallo, Z. Cao and D. Wang, *Appl. Catal. B- Environ.,* 247(2019)78.
32. N. Chen, Q. Mo, L. He, X. Huang, L. Yang, J. Zeng and Q. Gao, *Electrochim. Acta*, 299(2019)708.

33. Z. H. Zhao, F. Qin, S. Kasiraju, L. X. Xie, M. K. Alam, S. Chen, D. Z. Wang, Z. F. Ren, Z. M. Wang, L. C. Grabow and J. M. Bao, *ACS Catal.,* 7(2017)7312.
34. H. L. Lin, N. Liu, Z. P. Shi, Y. L. Guo, Y. Tang and Q. S. Gao, *Adv. Funct. Mater.,* 26(2016)5590.
35. Z. J, Zhao, W. Y. Chen, W. P. Li, X. D. Liang, H. Yan, X. Wang, J. C. Huang and M. Wu, *J. Mater. Res. Technol.*, 15(2021)2221.